





Angular distribution parameters in two-photon double ionization of helium beyond the dipole approximation

Yong-Kang Fang ¹, Hao Liang ¹, Wei-Chao Jiang ^{2,*}, and Liang-You Peng ^{1,3,4,5,†}

¹State Key Laboratory for Mesoscopic Physics and Frontiers Science Center for Nano-optoelectronics, School of Physics, Peking University, 100871 Beijing, China

²College of Physics and Optoelectronic Engineering, Shenzhen University, Shenzhen 518060, China

³Collaborative Innovation Center of Quantum Matter, Beijing 100871, China

⁴Collaborative Innovation Center of Extreme Optics, Shanxi University, 030006 Taiyuan, China

⁵Beijing Academy of Quantum Information Sciences, Beijing 100193, China



(Received 18 August 2021; revised 8 November 2021; accepted 16 December 2021; published 10 January 2022)

We study nondipole effects in the two-photon double ionization of helium by solving the full-dimensional time-dependent Schrödinger equation (TDSE). The angular distributions of the photoelectrons in TDSE calculations are parametrized by several angular distribution parameters. The electron correlation effects are revealed and discussed by analyzing angular distribution parameters of the photoelectrons. Compared with the linearly polarized laser, the values of dipole angular parameters for circularly polarized laser pulses in the nonsequential double-ionization regime are closer to the pure dipole emission of the one-photon single ionization, which indicates a weaker electron correlation for circular pulses. For the nondipole angular parameters, in the sequential double-ionization regime, we find that the parameters show peak structures from the sequential ionization channel over the energy sharing between two electrons and these peak positions are slightly shifted by the electron correlation. In general, due to the nondipole effects, the angular distributions of photoelectrons are shifted towards the direction of laser propagation, due to the transfer of the photon linear momentum.

DOI: [10.1103/PhysRevA.105.013104](https://doi.org/10.1103/PhysRevA.105.013104)

I. INTRODUCTION

Photoionization of atom has been a long-lasting problem which has been extensively explored in various circumstances. With the development of intense XUV sources from high-order harmonic generation (HHG) [1,2] and free-electron lasers (FELs) [3–5], the ionization of atom by one-photon and two-photon absorption has been experimentally accessible. As a two-electron atom, helium atom provides a good platform to study the role of electron correlation, which is very important in multielectron systems. After several decades of investigations, the one-photon double ionization (PDI) of helium has been well understood [6]. Three mechanisms have been proposed, i.e., the shake-off mechanism, the knock-out or two-step-one mechanism, and the quasifree mechanism from the quadrupole channel [7–10]. Recently, the research has been carried out by considering nondipole effects [11,12] including the momentum transfer from photon to the electron and ion [13,14]. Except for the discussions on the nondipole effects in PDI, more recent efforts have been put on the more complex two-photon double ionization.

The two-photon double ionization (TPDI) of helium is usually divided into two regimes according to the photon energy in the long laser pulse limit. For photon energy $39.5 \text{ eV} < \hbar\omega < 54.4 \text{ eV}$, TPDI can occur by simultaneously absorbing two photons. TPDI in this energy regime is called the nonsequential double ionization (NSDI) while, for photon energy

$\hbar\omega > 54.4 \text{ eV}$, the TPDI can be regarded as a result of two sequential one-photon absorption. It is called the sequential double ionization (SDI) in this energy regime. Though many computation results for the total cross section have been provided [15–20], reliable experimental measurements are still lacking [21–24]. Except for the total cross section, the differential spectra regarding the energy distribution and the angular distribution of two photoelectrons have also been well studied under dipole approximation.

For the cases of long laser pulses, it has been found [25–27] that, in the NSDI regime, the energy spectrum shows a “U” shape while, in the SDI regime, two sequential peaks at energies $\hbar\omega - I_{p1}$ and $\hbar\omega - I_{p2}$ will appear, with $I_{p1} = 24.6 \text{ eV}$ and $I_{p2} = 54.4 \text{ eV}$ being the first and second ionization potential of helium, respectively. If the photon energy is large enough, sequential channels related to the excited state of He^+ will be also opened, resulting in more sequential peaks [26,27]. As for the angular distributions, in the NSDI regime, the two electrons tend to take the back-to-back ejection mode [25] while, in the SDI regime, they show more complex structures. Near the sequential peaks, the photoelectrons tend to emit independently. For electron energies between the two main sequential peaks, they tend to take the back-to-back ejection mode while, for electron energies outside the main sequential peaks, they tend to be emitted in the same direction [27].

For the cases of short laser pulses, the distinction between NSDI and SDI by the photon energy becomes ambiguous. In the SDI regime for long laser pulses, the second ionization can occur a long time after the first ionization when the

*jiang.wei.chao@szu.edu.cn

†liangyou.peng@pku.edu.cn

electron correlation is negligible. However, in cases of short laser pulses, electrons are ionized at almost the same time. The electron correlation between them is not negligible. It has been found that the two main sequential peaks in the SDI regime in these cases will be closer to each other [28] and even become a single peak by shortening the laser pulses [29]. And electrons in the SDI regime will become more likely to take a back-to-back ejection mode as in the NSDI regime. Besides, Fomouo *et al.* [30] found that the two electrons in the NSDI regime of ultrashort laser pulses tend to absorb one photon individually and the U shape of energy spectrum also changes into an inverse U shape. All these signatures in short laser pulses suggest the idea that the distinction between NSDI and SDI becomes small. And the successful use of the virtual sequential picture for NSDI [31] also confirms this fact.

The angular distributions of photoelectrons are usually described by several asymmetric parameters. For the one-photon single ionization (PSI), angular distribution parameters have been derived including the nondipole terms [32] and several parameters were computed for the rare-gas atom [33]. For the one-photon double ionization, studies have also been made beyond the dipole approximation [34]. However, things become different for the two-photon process. Two-photon single ionization of halogen negative ions within the lowest-order perturbation theory under the dipole approximation was studied in Ref. [35]. And, recently, helium was also studied by solving the full-dimensional TDSE [36] while, for TPDI, there are two different ways to extract the angular distribution parameters. One is to extract angular distribution parameters of a single electron from the final double electron distribution. In this method, the indistinguishability of two electrons is considered and it is useful in both the SDI and NSDI regimes [26,37,38]. The second way is only useful in the SDI regime, which can be treated as the combination of two PSI processes, and the idea of PSI can be directly used. The angular distribution parameters for the two electrons are different [39–43]. In the second method, nondipole effects can be easily added. For the first method, however, like almost all existing studies for TPDI of helium, they are based on the dipole approximation, which means a unified description of the nondipole angular distribution in the NSDI regime and SDI regime has not been reached yet.

In this work, we will add nondipole corrections to the existing TPDI studies by solving the full-dimensional TDSE. Except for the dipole approximation and several works based on the elliptical or circular polarization laser pulse recently [44–47], most of the existing studies of TPDI have been based on the assumption of the linearly polarized laser pulse [16,25,26,28,29,48,49]. Here we will carry out the studies in the case of the elliptical and circular polarization. In order to study the role of electron correlation from the NSDI regime to SDI regime, we limit the photon energy from 40 eV to 100 eV, which is different from the photon energy used in experiment to measure the nondipole effect recently in the PSI of helium [50]. In particular, we will focus on the angular distribution parameters evaluated through the first method. Compared with linearly polarized laser pulses, the values of dipole angular parameters in the NSDI regime are closer to the pure dipole emission of PSI for circularly polarized laser pulses, which indicates a weaker electron correlation for

circular pulses. Based on the nondipole angular parameters, a newly defined relatively asymmetric parameter is used to describe the angular distributions of photoelectrons. The peak structures from the sequential ionization channel are found and the peak positions are shifted by the electron correlation. Through the reconstruction of angular distributions by angular distribution parameters, one finds electrons are shifted along the direction of laser propagation.

The rest of this paper is organized as follows. In Sec. II, we introduce our methods in detail and present the expressions of angular distribution parameters. We will present the dipole angular parameters in a way without the dependence on choice of particular frame of coordinates in order to compare our results with previous ones. In Sec. III, we will show our results of angular distribution parameters and give the explanation of the behavior of these parameters and, in Sec. IV, we will give a brief summary. Atomic units are used unless otherwise specified.

II. THEORETICAL METHODS

In this section, we present a brief introduction for our theoretical method to treat TPDI. Our method is based on the numerical solution of the full-dimensional TDSE of the two-electron system interacting with laser pulses beyond the dipole approximation. After the end of the laser pulses, the wave function is further propagated until the electron correlation can be neglected, and then the wave function is projected to the product of two Coulomb waves. Finally, we can extract observables such as the energy spectrum, angular distribution, and so on. In subsection A, we show how to solve the TDSE. In subsection B, we show how to extract the angular distribution parameters through the final wave function and give a brief discussion about the parameters. In subsection C, we present the form of the dipole angular parameters independent of coordinates. And we will provide the relationship between the values of parameters in different frames of coordinates.

A. Time-dependent Schrödinger equation

The TDSE of the two-electron system in a laser field can be written as

$$i \frac{\partial}{\partial t} \Psi(\mathbf{r}_1, \mathbf{r}_2, t) = H \Psi(\mathbf{r}_1, \mathbf{r}_2, t), \quad (1)$$

in which \mathbf{r}_1 and \mathbf{r}_2 are the coordinates of two electrons and H is the full Hamiltonian, which is given by

$$H = H_0 + H_I, \quad (2)$$

where H_0 is the Hamiltonian for the field-free helium atom and H_I is the interaction term between helium and laser pulse. H_0 can be written as

$$H_0 = \frac{\mathbf{p}_1^2}{2} + \frac{\mathbf{p}_2^2}{2} - \frac{2}{r_1} - \frac{2}{r_2} + \frac{1}{|\mathbf{r}_1 - \mathbf{r}_2|}, \quad (3)$$

where \mathbf{p}_1 and \mathbf{p}_2 are the momentum operators of the two electrons. In this work, we adopt the length gauge for H_I . In the dipole approximation, the laser pulse is only a function of time. By considering the first-order nondipole corrections, H_I

can be given by [14]

$$H_I = \sum_{i=1,2} \mathbf{r}_i \cdot \mathbf{E}(t) - \frac{\alpha}{2} (\hat{\mathbf{k}} \cdot \mathbf{r}_i) \left(\mathbf{r}_i \cdot \frac{\partial \mathbf{E}(t)}{\partial t} \right) + \frac{\alpha}{2} \mathbf{I}_i \cdot (\hat{\mathbf{k}} \times \mathbf{E}(t)), \quad (4)$$

where α , $\mathbf{E}(t)$, and $\hat{\mathbf{k}}$, are the fine-structure constant, electric-field vector, and the unit vector of propagation direction of laser pulses, and \mathbf{I}_1 , \mathbf{I}_2 are the angular momentum operators of the two electrons. In Eq. (4), the first term is the electric dipole term, the second term is the electric quadrupole term, and the last term is the magnetic dipole term.

In order to solve Eq. (1), we expand the wave function by

$$\Psi(\mathbf{r}_1, \mathbf{r}_2, t) = \sum_{L,M,l_1,l_2} \frac{R_{l_1 l_2}^{LM}(r_1, r_2, t)}{r_1 r_2} Y_{l_1 l_2}^{LM}(\hat{\mathbf{r}}_1, \hat{\mathbf{r}}_2), \quad (5)$$

in which

$$Y_{l_1 l_2}^{LM}(\hat{\mathbf{r}}_1, \hat{\mathbf{r}}_2) = \sum_{m_1, m_2} \langle l_1 m_1 l_2 m_2 | LM l_1 l_2 \rangle Y_{l_1}^{m_1}(\hat{\mathbf{r}}_1) Y_{l_2}^{m_2}(\hat{\mathbf{r}}_2), \quad (6)$$

where $\langle l_1 m_1 l_2 m_2 | LM l_1 l_2 \rangle$ is the Clebsch-Gordan coefficient. By assuming the laser is polarized in the x - y plane and propagates along the z direction, the vector potential of the laser pulse has the form

$$\mathbf{A}(t) = A_0 f(t) \left(\frac{1}{\sqrt{1+\epsilon^2}} \cos \omega t \mathbf{e}_x + \frac{\epsilon}{\sqrt{1+\epsilon^2}} \sin \omega t \mathbf{e}_y \right), \quad (7)$$

where $f(t)$ is the envelope of the laser pulse, which in the present work is given by $f(t) = \sin^2(\pi \frac{t}{\tau} + \pi/2)$ with τ being the total pulse duration, and ϵ is set to 1 for circularly polarized laser pulses.

For radial functions $R_{l_1 l_2}^{LM}(r_1, r_2, t)$ in Eq. (5), we employ the finite element discrete variable representation (FE-DVR) method, which has been successfully used in many studies of few-electron atoms and molecules interacting with laser pulses [51–55]. For the wave-function propagation, we use the Arnoldi propagator.

B. Angular distribution parameter

After a sufficiently long free propagation of the wave function, we project the final wave function to the double-ionization state which is constructed by the product of two one-electron Coulomb scattering states, which is given by

$$|\Psi_{DI}(\mathbf{k}_1, \mathbf{k}_2)\rangle = \frac{1}{\sqrt{2}} \left[|\psi_{\mathbf{k}_1}^{(-)}(\mathbf{r}_1)\rangle |\psi_{\mathbf{k}_2}^{(-)}(\mathbf{r}_2)\rangle + |\psi_{\mathbf{k}_1}^{(-)}(\mathbf{r}_2)\rangle |\psi_{\mathbf{k}_2}^{(-)}(\mathbf{r}_1)\rangle \right], \quad (8)$$

where $|\psi_{\mathbf{k}}^{(-)}(\mathbf{r})\rangle$ is the one-electron Coulomb scattering state [56]

$$|\psi_{\mathbf{k}}^{(-)}(\mathbf{r})\rangle = \frac{1}{\sqrt{2\pi k}} \sum_{l,m} i^l e^{-i(\sigma_l + \delta_l)} [Y_l^m(\hat{\mathbf{k}})]^* \tilde{R}_{k,l}(r) Y_l^m(\hat{\mathbf{r}}), \quad (9)$$

with

$$\tilde{R}_{k,l}(r) = \frac{2}{r} \frac{2^l e^{\pi Z/2k} |\Gamma(l+1+i\kappa)|}{(2l+1)!} e^{-ikr} (kr)^{l+1} \times {}_1F_1(l+1-i\kappa, 2l+2, 2ikr). \quad (10)$$

For the Coulomb potential, $\sigma_l = \arg \Gamma(l+1+i\kappa)$ and $\delta_l = 0$. Besides, ${}_1F_1$ is the Kummer confluent hypergeometric function and $\kappa = -\frac{Z}{k}$, where Z is the nuclear charge number and is set to 2 for TPDI of helium.

Then the differential momentum spectrum of the two electrons can be computed by

$$P(\mathbf{k}_1, \mathbf{k}_2) = \frac{k_1^2 k_2^2}{2} |\langle \Psi_{DI}(\mathbf{k}_1, \mathbf{k}_2) | \Psi(\mathbf{r}_1, \mathbf{r}_2, t_f) \rangle|^2 = \frac{1}{4\pi^2} \left| \sum_{L,M,l_1,l_2} Y_{l_1 l_2}^{L,M}(\hat{\mathbf{k}}_1, \hat{\mathbf{k}}_2) M_{l_1 l_2}^{L,M}(k_1, k_2) \right|^2, \quad (11)$$

with $M_{l_1 l_2}^{L,M}(k_1, k_2)$ given by

$$M_{l_1 l_2}^{L,M}(k_1, k_2) = (-i)^{l_1+l_2} e^{i(\delta_{l_1} + \delta_{l_2} + \sigma_{l_1} + \sigma_{l_2})} \times \int r_1 dr_1 \int r_2 dr_2 \tilde{R}_{k_1, l_1}(r_1) \tilde{R}_{k_2, l_2}(r_2) \times R_{l_1 l_2}^{L,M}(r_1, r_2, t_f). \quad (12)$$

The differential spectrum can be directly written as

$$P(E_1, E_2, \hat{\mathbf{k}}_1, \hat{\mathbf{k}}_2) = \frac{1}{k_1 k_2} P(\mathbf{k}_1, \mathbf{k}_2), \quad (13)$$

with $E_1 = k_1^2/2$ and $E_2 = k_2^2/2$.

Integrating over the variables θ_2 , φ_2 , φ_1 , we get

$$P(E_1, E_2, \theta_1) = \frac{1}{4\pi^2 k_1 k_2} \sum_{L,M,l_1,l_2} \sum_{L',M',l'_1,l'_2} \times [M_{l'_1 l'_2}^{L',M'}(k_1, k_2)]^* M_{l_1 l_2}^{L,M}(k_1, k_2) \times \sum_j \frac{2j+1}{2} \Pi_1(j) \begin{pmatrix} L & L' & j \\ -M & M' & 0 \end{pmatrix} \times P_j(\cos \theta_1), \quad (14)$$

with

$$\Pi_1(j) = (-1)^{l_2+M} \sqrt{(2l_1+1)(2l'_1+1)(2L+1)(2L'+1)} \times \delta_{l_2, l'_2} \begin{pmatrix} j & l'_1 & l_1 \\ 0 & 0 & 0 \end{pmatrix} \begin{Bmatrix} L & L' & j \\ l'_1 & l_1 & l_2 \end{Bmatrix}. \quad (15)$$

By defining

$$\beta_j(E_1, E_2) = \frac{\sqrt{(2j+1)\pi}}{4\pi^2 k_1 k_2} \sum_{L,M,l_1,l_2} \sum_{L',M',l'_1,l'_2} \times [M_{l'_1 l'_2}^{L',M'}(k_1, k_2)]^* M_{l_1 l_2}^{L,M}(k_1, k_2) \Pi_1(j, 0), \quad (16)$$

with

$$\begin{aligned} \Pi_1(j, m) &= \Pi_1(j) \sqrt{\frac{2j+1}{4\pi}} \begin{pmatrix} L & L' & j \\ -M & M' & m \end{pmatrix} \delta_{M, M'+m} \\ &= \langle l_1 l_2 L M | Y_j^m(\theta_1, \varphi_1) | l_1' l_2' L' M' \rangle, \end{aligned} \quad (17)$$

the angular distribution $P(E_1, E_2, \theta_1)$ can be written as

$$P(E_1, E_2, \theta_1) = \sum_j \beta_j(E_1, E_2) P_j(\cos \theta_1). \quad (18)$$

Integrating with respect to E_2 and comparing our angular distribution parameters with that in PSI or PDI [32,34], we can get

$$\begin{aligned} P(E_1, \theta_1) &= \sum_j \beta_j(E_1) P_j(\cos \theta_1) \\ &= \frac{\sigma_0(E_1)}{2} \left\{ 1 + \tilde{\beta}_2(E_1) P_2(\cos \theta_1) \right. \\ &\quad + \left[\delta(E_1) + \frac{1}{2} \gamma(E_1) \sin^2(\theta_1) \right] \cos(\theta_1) \\ &\quad \left. + \tilde{\beta}_4(E_1) P_4(\cos \theta_1) + \tilde{\beta}_5(E_1) P_5(\cos \theta_1) \right\}, \end{aligned} \quad (19)$$

with

$$\begin{aligned} \beta_j(E_1) &= \int dE_2 \beta_j(E_1, E_2), \\ \sigma_0(E_1) &= 2\beta_0(E_1), \\ \tilde{\beta}_j(E_1) &= \frac{\beta_j(E_1)}{\beta_0(E_1)}, \\ \gamma(E_1) &= -5\tilde{\beta}_3(E_1), \\ \delta(E_1) &= \tilde{\beta}_1(E_1) + \tilde{\beta}_3(E_1). \end{aligned} \quad (20)$$

In the present work, we compute the angular distribution parameters until $j = 5$, which is reasonable and will be explained below.

These angular distribution parameters can be divided into two groups—dipole angular parameters and nondipole angular parameters. If we use the dipole approximation, only the dipole parameters will appear and all nondipole parameters will be equal to zero. The parameters can be divided into these two groups under the following analysis.

(i) At first, the initial state of helium atom is a ground state with $L^i = M^i = 0$ and $l_1^i = l_2^i$ (i represents the initial state).

(ii) For one-photon absorption, the selection rule for the electric dipole limits $\Delta l_1 = \pm 1$ or $\Delta l_2 = \pm 1$. For the electric quadrupole, the selection rule limits $\Delta l_1 = \pm 2, 0$ or $\Delta l_2 = \pm 2, 0$ and, for the magnetic dipole, it limits $\Delta l_1 = \Delta l_2 = 0$.

(iii) Considering the first-order small quantity, the final state in TPDI can be reached through two dipole channels (path A), or one dipole channel and one nondipole channel (path B). For path A, $(l_1^f + l_2^f)$ is an even number while it is an odd number for path B (f represents the final state). For path A, $L_{\max}^f = 2$ and, for path B, $L_{\max}^f = 3$.

(iv) According to Eqs. (15), (16), and (17), if the angular distribution parameter is not equal to zero, $(j + l_1' + l_1)$ should be an even number and $l_2' = l_2$ with two final partial waves (L, M, l_1, l_2) and (L', M', l_1', l_2') , which also means

$(j + l_1' + l_1 + l_2' + l_2)$ is an even number. The two final partial waves should be both from path A, or one from path A and another from path B in the limit of considering the first order small quantity. If two final partial waves are both from path A, $(l_1' + l_1 + l_2' + l_2)$ is an even number and j is also an even number. If two final partial waves are not both from path A, $(l_1' + l_1 + l_2' + l_2)$ is an odd number and j is also an odd number.

(v) Finally, we know that all even order angular distribution parameters should be dipole angular parameters and all odd order distribution parameters are nondipole angular parameters.

(vi) According to the requirement that L , L' , and j should form a triangle, the maximum of j should be taken to be 5.

C. Angular distribution parameters in different frames of coordinates

For linear polarization of laser pulses, one usually assumes it polarizes in the z direction and propagates in the x or y direction. This coordinate frame will be called Σ below. But for circular or elliptical polarization of laser pulses, one usually assumes it propagates along the z direction with the pulse polarization in the x - y plane, which will be denoted as Σ_0 below. Although the physics does not depend on the choice of the framework of coordinates, the values of observables will be different. To confirm the validity and accuracy of our computation, we derive the relationships of dipole angular parameters between different frames of coordinates. The dipole approximation is used below because only dipole angular parameters have been computed in literature.

According to Ref. [57], in TPDI, the transition matrix element can be written as

$$\begin{aligned} F(\mathbf{k}_1, \mathbf{k}_2) &= f_1(\hat{\mathbf{k}}_1 \cdot \mathbf{e})^2 + f_2(\hat{\mathbf{k}}_2 \cdot \mathbf{e})^2 \\ &\quad + f_s(\hat{\mathbf{k}}_1 \cdot \mathbf{e})(\hat{\mathbf{k}}_2 \cdot \mathbf{e}) + f_0(\mathbf{e} \cdot \mathbf{e})^2, \end{aligned} \quad (21)$$

in which f_1, f_2, f_s, f_0 are the functions of $E_1, E_2, \hat{\mathbf{k}}_1 \cdot \hat{\mathbf{k}}_2$, and \mathbf{e} is the polarization direction of the electric field. Similar to Ref. [37], we define $N_1^{k_1} = 2, N_1^{k_2} = 0, N_2^{k_1} = 0, N_2^{k_2} = 2, N_s^{k_1} = N_s^{k_2} = 1, N_0^{k_1} = N_0^{k_2} = 0$; then the final distribution of two electrons in the momentum space is given by

$$\begin{aligned} P(\mathbf{k}_1, \mathbf{k}_2) &\propto |F(\mathbf{k}_1, \mathbf{k}_2)|^2 \\ &= \sum_{i,j} f_i f_j^* (\hat{\mathbf{k}}_1 \cdot \mathbf{e})^{N_i^{k_1} + N_j^{k_1}} (\hat{\mathbf{k}}_2 \cdot \mathbf{e})^{N_i^{k_2} + N_j^{k_2}}, \end{aligned} \quad (22)$$

with $i, j = 1, 2, s, 0$. $f_i f_j^*$ can be expanded by

$$f_i f_j^* = \sum_l B_l P_l(\hat{\mathbf{k}}_1 \cdot \hat{\mathbf{k}}_2), \quad (23)$$

where B_l is the coefficient of $P_l(\hat{\mathbf{k}}_1 \cdot \hat{\mathbf{k}}_2)$ and it is a function of E_1, E_2 . By using the equation for the Legendre function,

$$\int d\Omega_{\hat{\mathbf{k}}_2} P_l(\hat{\mathbf{k}}_1 \cdot \hat{\mathbf{k}}_2) P_l(\hat{\mathbf{k}}_2 \cdot \mathbf{e}) = 4\pi(2l+1)^{-1} P_l(\hat{\mathbf{k}}_1 \cdot \mathbf{e}) \delta_{ll'}, \quad (24)$$

and integrating with respect to \mathbf{k}_2 , we get

$$\frac{d\sigma}{dE_1 d\Omega_1} \propto \sum_{l=0}^4 C_l(E_1) P_l(\hat{\mathbf{k}}_1 \cdot \mathbf{e}), \quad (25)$$

in which $C_l(E_1)$ is the coefficient. Note that l can only be 0, 2, and 4, consistent with the discussion above for angular parameters. Actually, this constraint for l can also be derived from equations above. First, according to Eqs. (22), (24), and (25), the value of l in Eq. (25) has the same parity with $(N_i^{k_1} + N_j^{k_1} + N_i^{k_2} + N_j^{k_2})$ and is not larger than its maximum. According to the definition of these values, it can only be an even number and its maximum value is 4. So l in Eq. (25) can only take 0, 2, and 4. Then we can change Eq. (25) to

$$\frac{d\sigma}{dE_1 d\Omega_1} = \frac{d\sigma}{dE_1} \left(1 + \alpha_2 P_2(\hat{\mathbf{k}}_1 \cdot \mathbf{e}) + \alpha_4 P_4(\hat{\mathbf{k}}_1 \cdot \mathbf{e}) \right), \quad (26)$$

with α_2, α_4 being the angular distribution parameters. It is obvious that these expressions are independent of the frame of coordinates and can be used to provide a connection between different coordinates. We will present them for the cases of the linear polarization and the circular polarization in coordinate systems of Σ and Σ_0 below. We would like to point out that, in the next discussion for the linear polarization and the circular polarization, θ is the angle between z axis and \mathbf{k} and φ is the angle between x axis and the projection of \mathbf{k} in the x - y plane in both frames of coordinates Σ and Σ_0 .

1. Linearly polarized laser pulses

For linearly polarized laser pulses, one usually chooses the coordinate Σ . In Eq. (26), with $\hat{\mathbf{k}}_1 \cdot \mathbf{e} = \cos \theta_1$, one can directly get α_2 and α_4 . For the coordinate Σ_0 , the laser is polarized along the x direction; thus one has $\hat{\mathbf{k}}_1 \cdot \mathbf{e} = \sin \theta_1 \cos \varphi_1$. Inserting this into Eq. (26) and integrating over φ_1 , we get

$$\frac{d\sigma}{dE_1 d\theta_1} = \frac{d\sigma}{dE_1} \left(1 - \frac{1}{2} \alpha_2 P_2(\cos \theta_1) + \frac{3}{8} \alpha_4 P_4(\cos \theta_1) \right). \quad (27)$$

However, according to Eq. (19), what one directly gets are $\tilde{\beta}_2$ and $\tilde{\beta}_4$ in Σ_0 . Therefore, one arrives at the following relation:

$$\tilde{\beta}_2 = -\frac{1}{2} \alpha_2, \quad (28)$$

$$\tilde{\beta}_4 = \frac{3}{8} \alpha_4, \quad (29)$$

which connects angular distribution parameters in different coordinates (Σ , Σ_0) for linearly polarized laser pulses.

2. Circularly polarized laser pulses

For circularly polarized laser pulses, the electric field changes with time; under the time averaging one has the relation that $\langle (\hat{\mathbf{k}}_1 \cdot \mathbf{e})^2 \rangle_T = \frac{1}{2} \sin^2 \xi$ and $\langle (\hat{\mathbf{k}}_1 \cdot \mathbf{e})^4 \rangle_T = \frac{3}{8} \sin^2 \xi$, with ξ being the angle between \mathbf{k}_1 and the propagation direction of laser pulses. In Σ_0 , the pulse propagates along the z axis and thus $\xi = \theta_1$, which leads to

$$\langle P_2(\hat{\mathbf{k}}_1 \cdot \mathbf{e}) \rangle_T = -\frac{1}{2} P_2(\cos \theta_1), \quad (30)$$

$$\langle P_4(\hat{\mathbf{k}}_1 \cdot \mathbf{e}) \rangle_T = \frac{3}{8} P_4(\cos \theta_1). \quad (31)$$

Inserting the above relations into Eq. (26) and integrating over φ_1 , we get

$$\frac{d\sigma}{dE_1 d\theta_1} = \frac{d\sigma}{dE_1} \left[1 - \frac{1}{2} \alpha_2 P_2(\cos \theta_1) + \frac{3}{8} \alpha_4 P_4(\cos \theta_1) \right]. \quad (32)$$

Again, in Σ_0 , what one directly gets are $\tilde{\beta}_2$ and $\tilde{\beta}_4$, so the relations between them are given by

$$\tilde{\beta}_2 = -\frac{1}{2} \alpha_2, \quad (33)$$

$$\tilde{\beta}_4 = \frac{3}{8} \alpha_4. \quad (34)$$

One can find that the relations of angular distribution parameters in different frames of coordinates are the same for the linear and the circular polarization laser pulse. Further, one can prove that the relations are independent of the ellipticity of the laser field.

Before we close this section, we would like to point out that, in Sec. III, the energy sharing between the two electrons ($\eta = \frac{E_1}{E_1 + E_2}$) and the total energy ($E = E_1 + E_2$) of the two electrons are used as variables rather than E_1, E_2 . Expressed in terms of the variables η and E , the angular distribution is given by

$$P(E, \eta, \theta_1) = \sum_j \beta_j(E, \eta) P_j(\cos \theta_1), \quad (35)$$

with $\beta_j(E, \eta) = E \beta_j(E_1, E_2)$. Integrating with respect to E and recombining the parameters, we get

$$\begin{aligned} P(\eta, \theta_1) &= \sum_j \beta_j(\eta) P_j(\cos \theta_1) \\ &= \frac{\sigma_0(\eta)}{2} \left\{ 1 + \tilde{\beta}_2(\eta) P_2(\cos \theta_1) \right. \\ &\quad \left. + \left[\delta(\eta) + \frac{1}{2} \gamma(\eta) \sin^2(\theta_1) \right] \cos(\theta_1) \right. \\ &\quad \left. + \tilde{\beta}_4(\eta) P_4(\cos \theta_1) + \tilde{\beta}_5(\eta) P_5(\cos \theta_1) \right\}, \quad (36) \end{aligned}$$

with

$$\begin{aligned} \beta_j(\eta) &= \int dE \beta_j(E, \eta), \\ \sigma_0(\eta) &= 2\beta_0(\eta), \\ \tilde{\beta}_j(\eta) &= \frac{\beta_j(\eta)}{\beta_0(\eta)}, \\ \gamma(\eta) &= -5\tilde{\beta}_3(\eta), \\ \delta(\eta) &= \tilde{\beta}_1(\eta) + \tilde{\beta}_3(\eta). \quad (37) \end{aligned}$$

Apparently, the angular distribution parameters expressed in E_1, E_2 or η, E have the same properties.

III. RESULTS

In this section, we will provide our main results of the angular distribution parameters. In subsection A, we focus

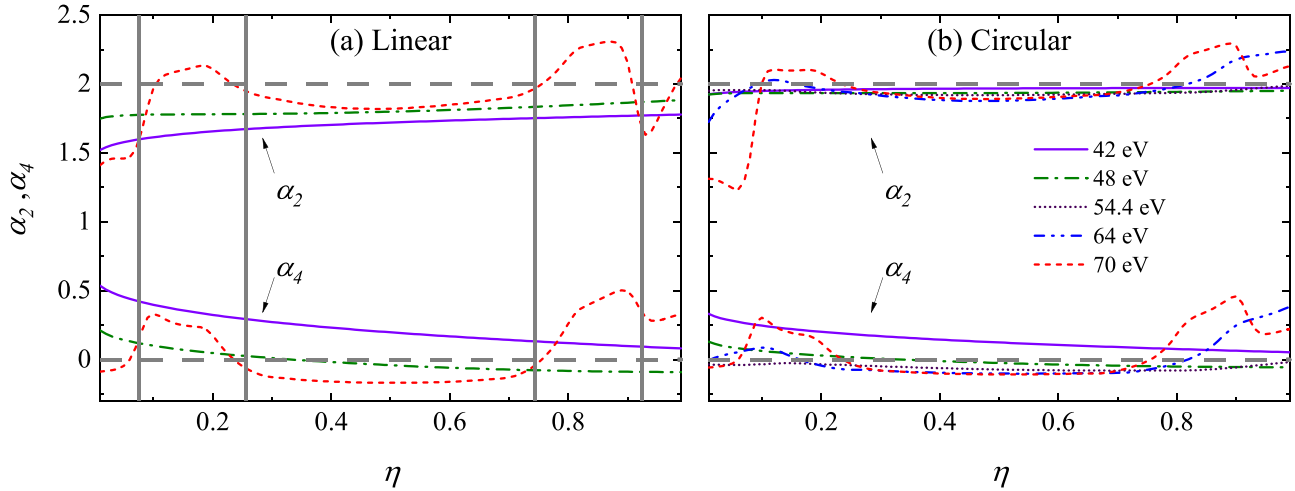


FIG. 1. Dipole angular parameters for a linearly (left panel) and circularly (right panel) polarized pulse for a duration of 2 fs at different photon energies. The two horizontal gray dashed lines at 2 and 0 in each panel represent the cases of an uncorrelated emission of electrons. The vertical gray solid lines are respectively related to the sequential process of the ground state of He^+ (the inner two) and the first excited state of He^+ (the outer two), for the case of 70 eV.

on the dipole angular parameters. At first, dipole parameters for the linearly polarized pulses are compared with the existing results in literature. Then, we will present and discuss the dipole parameters for circularly polarized pulses. In subsection B, we will show and analyze the nondipole angular parameters via the features in the electron angular distributions. In subsection C, we provide the one-electron angular distribution, which is reconstructed by angular distribution parameters.

A. Dipole angular parameters

To check the validity of our results, we extract the angular distribution parameters $\tilde{\beta}_2, \tilde{\beta}_4$ under the dipole approximation with a linearly polarized laser pulse in the frame of coordinates Σ_0 . According to Eq. (28), the dipole angular parameters α_2, α_4 in coordinate Σ can be obtained.

The photon energies are chosen to be 42 eV, 48 eV, and 70 eV, respectively. Results are shown in Fig. 1(a). In Ref. [26], the dipole angular parameters α_2, α_4 are denoted as β, γ . In their calculations, the duration of the laser pulses τ is taken to be 4.5 fs and the maximal total angular momentum number L_{\max} and the maximal single electron angular momentum number l_{\max} are chosen to be 2 and 10, respectively. However, τ, L_{\max} , and l_{\max} are respectively set to be 2 fs, 4, and 5 in our calculations. Although the value of angular momentum number is different, the convergence of results is checked and ensured in our computation with the laser intensity of 10^{12} W/cm^2 . Comparing these two sets of results, we note that not only the trend of the parameters but also the values are identical. Nevertheless, there is a little difference when the photon energy is 70 eV. Our results do not change so acutely like theirs near the sequential threshold, shown by the vertical gray solid lines in Fig. 1(a). We think this is because we use a shorter duration of 2 fs, which results in a larger spectrum broadening. Then, we turn to the dipole angular parameters for circularly polarized laser pulses. According to Eq. (26), dipole angular parameters α_2, α_4 are shown in

Fig. 1(b). In the SDI regime, the main signature does not change in the case of the circular polarization. However, in the NSDI regime, compared with the results of the linear polarization, α_2 is closer to 2 and α_4 is closer to 0, which means that electrons are more likely to be emitted like PSI of the ground state of the hydrogen atom for the circularly polarized pulses. In fact, previous studies for ultrashort laser pulses in the NSDI regime [30] and the successful application of the virtual sequential picture for NSDI [31] also suggests that electrons tend to absorb one photon individually in the NSDI regime.

According to the above discussion, TPDI in the NSDI regime can be qualitatively understood by a simple physical picture. When the helium atom interacts with laser pulses, two electrons tend to absorb one photon individually. Neglecting the electron correlation, only one electron would be ionized for $I_{p1} < \omega < I_{p2}$. However, with the inclusion of the electron correlation, the second electron can be also ionized. At the same time, the electron correlation will result in a deviation of α_2, α_4 from 2,0, respectively. Compared with the case of the linear polarization, the electron correlation will be weaker and the deviation of α_2, α_4 will be correspondingly smaller for circular pulses. To further confirm this physical picture, results of dipole angular distribution parameters under different ellipticity of the laser field are shown for the NSDI regime (42 eV) in Fig. 2(a). It can be clearly seen that, when ϵ changes from 0 to 1, α_2 grows closer to 2 and α_4 grows closer to 0, which suggests the weaker electron correlation for a larger ellipticity of the laser field. This result is consistent with the physical picture above. Besides, we also show the dependence on ellipticity of the laser field in the SDI regime in Fig. 2(b). One can find that, when ϵ changes from 0 to 1, α_4 grows closer to 0. For α_2 , it grows closer to 2 when η does not reach the regime where the sequential process of the excited state of He^+ is open. All these results suggest that the larger ellipticity of the laser field leads to the weaker electron correlation in either the NSDI regime or the SDI regime. This conclusion can be partly seen in the study of the angular distribution in a

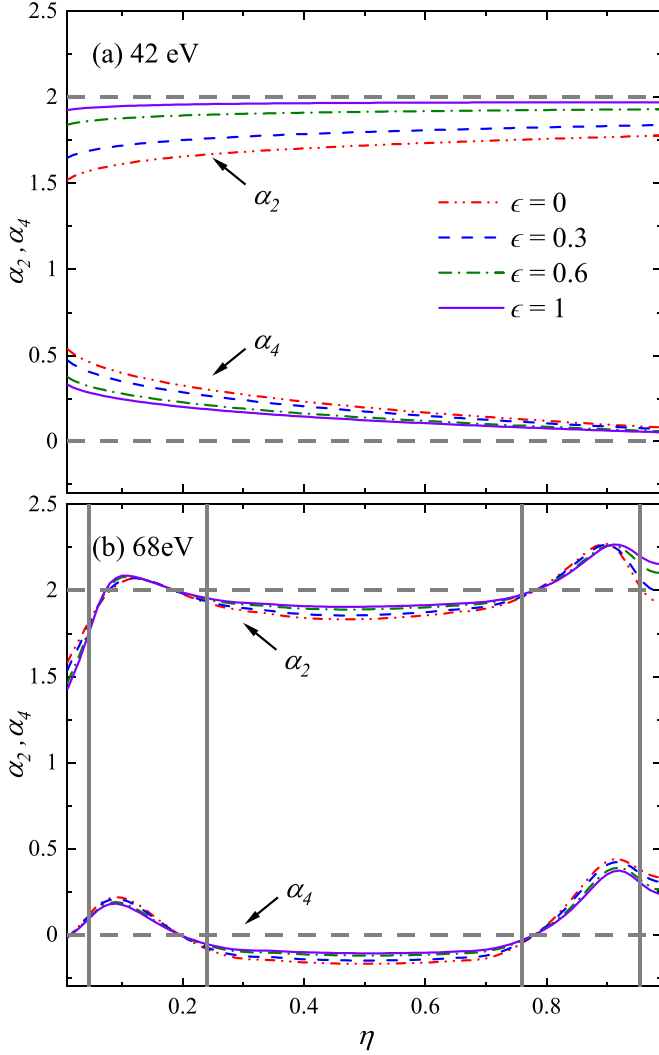


FIG. 2. Dipole angular distribution parameters for 42 eV (upper panel) and 68 eV (lower panel) under different ellipticity of the laser field. $\epsilon = 0$ (1) represents linear (circular) polarization laser pulse. Besides, the pulse duration is 2 fs for 42 eV and 20 cycles for 68 eV. The two horizontal gray dashed lines at 2 and 0 in each panel represent the cases of an uncorrelated emission of electrons. The vertical gray solid lines are respectively related to the sequential process of the ground state of He^+ (the inner two) and the first excited state of He^+ (the outer two), for the case of 68 eV.

fixed configuration of two photoelectrons with the ultrashort laser pulse in Ref. [47].

B. Nondipole angular parameters

Only a circularly polarized laser pulse is used to study the nondipole angular parameters because usually the coordinate frames are different for linearly and circularly polarized laser pulses as we discussed above and, unlike the dipole angular parameters, there is not a simple correlation for the values of nondipole angular parameters in different coordinate frames. In Fig. 3, we present the results of nondipole angular parameters γ , δ , $\tilde{\beta}_5$ with circularly polarized laser pulses in the frame of coordinate Σ_0 . The value of γ is about two orders of magnitude larger than that of δ and $\tilde{\beta}_5$, which means the nondipole contribution of the angular distribution of electron is dominated by γ . In the NSDI regime, when η increases, δ and $\tilde{\beta}_5$ are almost zero, while γ will increase from negative values to positive values quickly at first and then the increase will slow down. In general, γ is a concave function of η . In this paper, the concave function means that its second derivative is negative. This concave behavior acts like a background for γ in the SDI regime. For γ in the SDI regime, other features are the peaks on the background which are related to the sequential ionization process. Besides, the variation of γ , δ , $\tilde{\beta}_5$ is synchronous, which means the underlying physical origin is the same.

To understand the behavior of nondipole angular parameters, we define a relatively asymmetric parameter A , which is given by

$$A(\eta) = \frac{P_+(\eta) - P_-(\eta)}{P_+(\eta) + P_-(\eta)}, \quad (38)$$

with $P_+(\eta)$ and $P_-(\eta)$ given by

$$P_+(\eta) = \int_0^{\pi/2} P(\eta, \theta_1) \sin \theta_1 d\theta_1, \quad (39)$$

$$P_-(\eta) = \int_{\pi/2}^{\pi} P(\eta, \theta_1) \sin \theta_1 d\theta_1. \quad (40)$$

Note that $P_+(\eta)$ and $P_-(\eta)$ are respectively related to electron distribution along with and opposite to the laser propagation direction. Thus $A(\eta)$ stands for the extent of electron emission along the laser propagation direction. It can be easily shown that the asymmetric parameter A is related to the

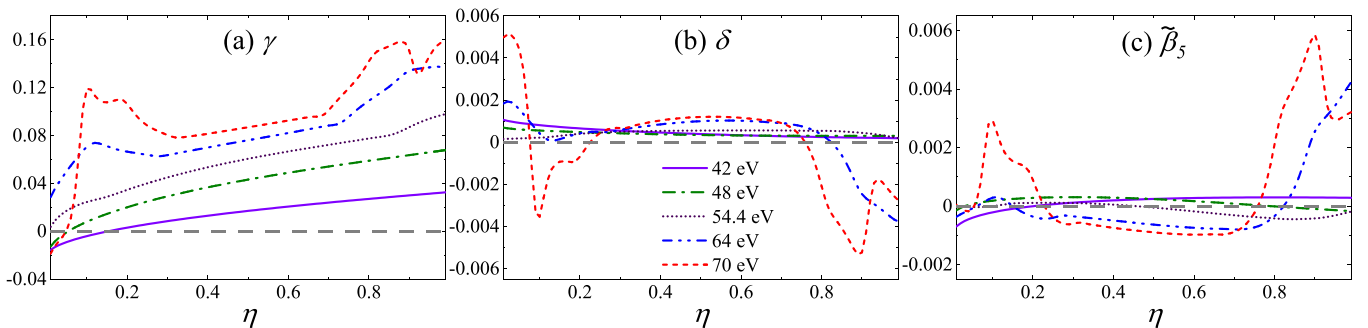


FIG. 3. Nondipole angular parameters γ , δ , and $\tilde{\beta}_5$ for a 2 fs pulse of circular polarization at different photon energies. The horizontal gray dashed line at zero represents the results if nondipole effects are not considered.

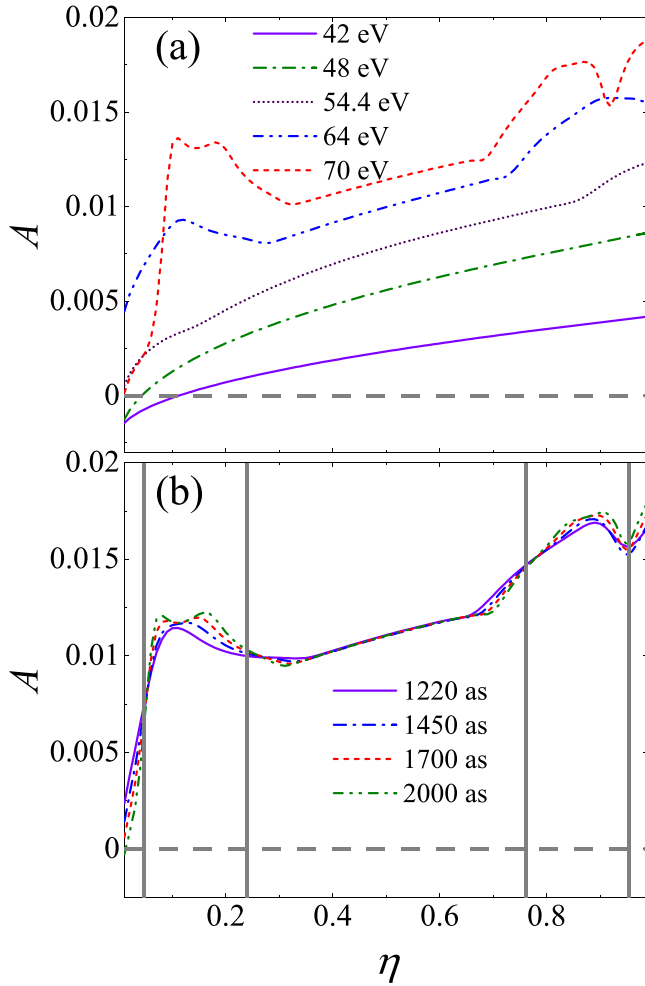


FIG. 4. Relatively asymmetric parameter A as a function of the energy sharing η for circularly polarized laser pulses. The horizontal gray dashed line at zero in each panel represents the results in the case where nondipole effects are not considered. (a) The duration of laser pulses is 2 fs, but for different photon energies. (b) The photon energy is fixed at 68 eV, but for different pulse durations. The vertical gray solid lines are related to the sequential process of the ground state of He^+ (the inner two) and the first excited state of He^+ (the outer two).

angular distribution parameters by

$$A = \frac{\delta}{2} + \frac{\gamma}{8} + \frac{\beta_5}{16} \approx \frac{\gamma}{8}. \quad (41)$$

Apparently, similar to γ , the relatively asymmetric parameter A is a concave function of η . In Fig. 4(a), we show results of A at different photon energies with a 2 fs circularly polarized laser pulse. When a photon interacts with an atom, it will transfer its linear momentum to the electron and the ion [58]. Intuitively, the electron will have a positive momentum along the laser propagation direction, which means A will be positive. However, the Coulomb effect from the nucleus will attract the electron to the nucleus, which results in the decrease of A . For the lower energy electron, the Coulomb interaction will be comparatively stronger. Therefore, A will be a concave function in general.

In the SDI regime, the relatively asymmetric parameter A (or equivalently γ) has several peaks on the concave background in Fig. 4(a). For photon energy of 64 eV, there are only two peaks while there are four peaks for 70 eV, although they tend to cluster together. These peaks may come from sequential TPDI channels. For 64 eV, the intermediate state can only be the ground state of He^+ for a monochromatic light. However, for an even larger photon energy, the channel of the first excited state of He^+ can be also opened, which results in four peaks in 70 eV with long enough laser pulses. In Fig. 4(b), we show the results of A with photon energy of 68 eV at different pulse durations. The positions of the standard channel of sequential TPDI of the ground state and the first excited state of He^+ are shown by vertical gray solid lines. For a short pulse duration of 1220 as including about 20-cycle oscillations, there are only two peaks. With the increase of the pulse duration to about 1700 as, the two peaks start to split into four peaks. However, the position of the peaks are not exactly at the position of the sequential channel. For the sequential channel related to the ground state of He^+ , the peaks move outward, while the peaks move inward for the sequential channel related to the excited state of He^+ .

The meaning of the relatively asymmetric parameter A in the SDI regime can be understood in another perspective. For the sequential TPDI process, the ionization process can be regarded as two PSI within the single-active electron approximation. According to the photon momentum transfer, both electrons will have a positive momentum along the laser propagation direction, which means that A is positive. This is confirmed in Fig. 4 near the sequential channel. Therefore, the value of A also stands for the extent of ejection of two electrons in the same direction. A larger value of A means that electrons are more likely to be emitted in the same direction.

Now let us turn to discussing the underlying mechanism of the shift of the peak positions in A , which may be related to the electron correlation. We denote the sequential TPDI process with the ground state of He^+ as g channel and the first excited state as e channel. For the g channel, if the electron correlation does not exist, the peaks of A should be exactly at the position η_1 and η_2 with $\eta_1 = \frac{\omega - I_{p1}}{2\omega - I_p}$ and $\eta_2 = \frac{\omega - I_{p2}}{2\omega - I_p}$, where $I_p = I_{p1} + I_{p2}$ is the ionization potential of helium. After the first electron (the fast one) is ionized through the g channel, the second electron (the slow one) will be ionized. If two electrons are ejected in the same direction, the electron correlation between them will tend to change the energy sharing to an extreme distribution, which is also called the postcollision interaction, while, if two electrons move in the opposite direction, for the fast electron, the screening of the core is reduced due to the ionization of the slow electron. The energy of the fast electron will decrease and the energy of the slow electron will increase, which will tend to change the energy distribution to an equal energy sharing. Therefore, electrons tend to be emitted in the opposite direction in the interval $\eta \in (\eta_2, \eta_1)$, while electrons outside this interval tend to be emitted in the same direction. The above observation has been found within the dipole approximation in Ref. [27]. Inside the energy interval, the value of A will be smaller than that in the region outside the interval. Therefore, the peak positions will shift outward.

For the e channel, the first ionized electron is the slow electron and the second ionized electron is the fast electron. Electrons tend to move in the same direction in the interval $\eta \in (\eta'_1, \eta'_2)$ with $\eta'_1 = \frac{\omega - I_{p1} - \Delta E}{2\omega - I_p}$ and $\eta'_2 = \frac{\omega - I_{p2} + \Delta E}{2\omega - I_p}$, where ΔE is the energy difference between the ground state and the excited state of He^+ . On the contrary, electrons outside the energy interval will tend to move in the opposite direction. This causes the peak positions of the e channel to shift inward. Therefore, in Fig. 4(b), one finds the deviation of peak positions from the sequential ionization threshold of A for long enough pulses. If the pulse duration decreases, electrons are more likely to be emitted in the opposite direction [29]. According to the discussion above, compared with the cases of long laser pulses, the peak of the g channel will move outward, while the peak of the e channel will move inward and the value of A will decrease. If the pulse duration is short enough, four peaks of the g channel and the e channel will merge into two peaks.

Finally, we will examine the value of A at point $\eta = 0$, which is shown in Fig. 4. In the NSDI regime, A is negative because of the attraction from the nucleus. In the SDI regime, governed by the sequential channel, the value is positive when the photon energy is just above I_{p1} . If one increases the photon energy, due to the spectrum broadening and electron correlation, the value of A gradually increases and is still governed by the sequential channel. When the sequential channel is far away from $\eta = 0$, A begins to decrease and is mainly governed by the Coulomb interaction from the nucleus. In this case, it even becomes negative again for long enough laser pulses.

C. Reconstruction of angular distribution

Through angular distribution parameters, one can reconstruct the one-electron angular distribution if one integrates over the variable η in Eq. (36). One expects that the angular distribution reconstructed by angular distribution parameters and that directly computed from the two-electron momentum distribution from TDSE should be exactly the same.

For circularly polarized pulses, in Fig. 5, we show results at two different photon energies of 42 eV and 68 eV in the NSDI regime and the SDI regime in the first and second row, respectively. In the left column of each case, we show the angular distributions of the electrons reconstructed from all the parameters (labeled with “total”) and only from the dipole parameters $\tilde{\beta}_2$ and $\tilde{\beta}_4$ (labeled with “dipole”). Apparently, the nondipole corrections to the angular distributions are larger for the 68 eV case and can merely be noticed with naked eyes, while the difference between the two results is hardly detectable for 42 eV. Further, the relative scale of the nondipole angular distribution and the dipole angular distribution is shown in Fig. 6. Clearly, one finds the nondipole correction is larger for larger photon energy. Besides, in the direction away from the polarization plane, the nondipole correction will be relatively important. Moreover, the ratio is antisymmetric under the transformation from θ to $\pi - \theta$ due to the symmetry of dipole and nondipole angular distribution. The positive (negative) value of the ratio represents the enhancement (reduction) of the angular distribution. Therefore, when the nondipole corrections are included, one can draw a conclusion that the angular distribution will be shifted right-

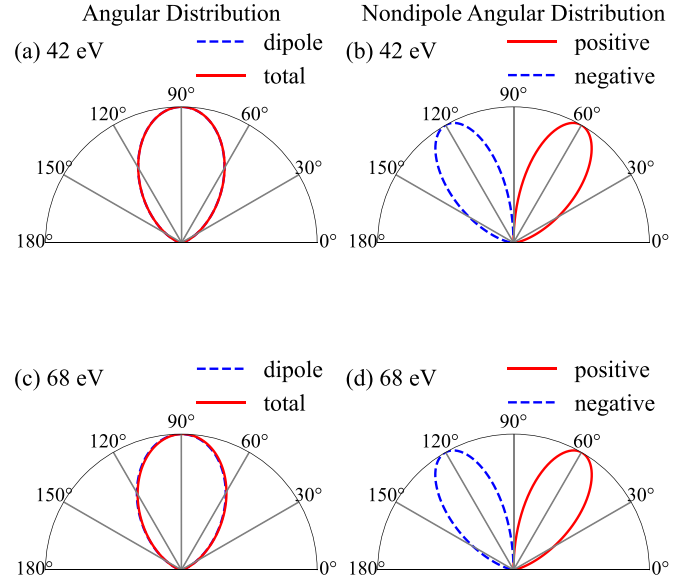


FIG. 5. Reconstructed one-electron angular distribution in the NSDI regime (the first row) and the SDI regime (the second row). The angle 0° represents the direction of the laser propagation. The left column represents distributions reconstructed by the dipole parameters only (dipole) and by all the parameters (total). The right column shows the angular distributions reconstructed only by the nondipole parameters.

ward along the direction of the laser propagation due to the photon linear momentum transfer to the ionized electron.

For a better illustration, in the right column of Fig. 5, we reconstruct the electron angular distributions that are solely contributed by the nondipole parameters γ , δ , and $\tilde{\beta}_5$. Consistent with the picture of the photon momentum transfer, the angular distribution is enhanced along the propagation direction of the laser pulse (labeled as “positive”), while it is reduced in the opposite direction of the laser propagation (labeled as “negative”).

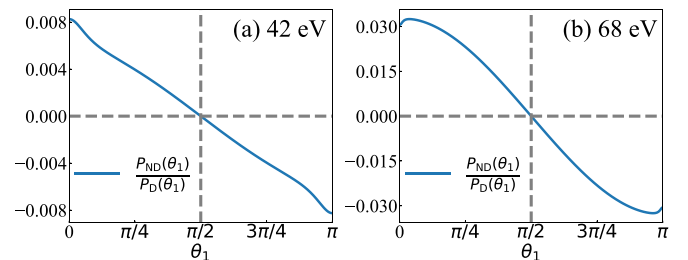


FIG. 6. Relative scale of nondipole angular distribution $P_{\text{ND}}(\theta_1)$ and the dipole angular distribution $P_{\text{D}}(\theta_1)$ with photon energy 42 eV (left panel) and 68 eV (right panel). The horizontal dashed gray line represents the value zero. The direction perpendicular to the propagation direction laser pulse is shown by the vertical dashed gray line. The positive (negative) value represents the enhancement (reduction) of the angular distribution because of nondipole corrections.

IV. SUMMARY

In conclusion, we have presented a detailed study of the two-photon double ionization of helium. In this work, we have focused the nondipole corrections to the parameters of the angular distribution of the electron for the cases of circularly polarized laser pulses. As shown, according to the different ionization channels, the angular distribution parameters can be divided into two groups—the dipole angular parameters and the nondipole angular parameters. Through the analysis of the behavior of these parameters in terms of the energy sharing, we discuss the effects of the electron correlation.

For the dipole angular parameters, in the NSDI regime, the values of parameters are closer to those from the pure dipole emission in PSI compared with the linear polarization case, which indicates a weaker electron correlation for NSDI by circularly polarized pulses.

For the nondipole angular parameters, the behavior of parameters as the function of the energy sharing becomes more complex, which can be better explained by defining a relatively asymmetric parameter A . Because of the Coulomb attraction from the nucleus, the behavior of A in the NSDI regime is a concave function of the energy sharing η . In

the SDI regime, there are some peaks of A related to the sequential ionization channels on the concave background. We have presented a detailed analysis of these peaks and their shifts, depending on different ionization channels and mutual interactions between the two electrons and the nucleus, as well as the duration of the laser pulse.

Through the angular distribution parameters, one-electron angular distribution is reconstructed. Comparing the total angular distribution and the dipole angular distribution, one can draw a conclusion that due to the momentum transfer electrons are shifted along the direction of laser propagation, which is further confirmed by the nondipole angular distribution.

ACKNOWLEDGMENTS

This work is supported by the National Natural Science Foundation of China Grants No. 11725416, No. 11961131008, No. 12074265, and No. 11804233 and by the National Key R&D Program of China Grant No. 2018YFA0306302.

-
- [1] M. Hentschel, R. Kienberger, C. Spielmann, G. Reider, N. Milosevic, T. Brabec, P. Corkum, U. Heinzmann, M. Drescher, and F. Krausz, *Nature (London)* **414**, 509 (2001).
 - [2] P. M. Paul, E. S. Toma, P. Breger, G. Mullot, F. Augé, P. Balcou, H. G. Muller, and P. Agostini, *Science* **292**, 1689 (2001).
 - [3] P. Emma, R. Akre, J. Arthur, R. Bionta, C. Bostedt, J. Bozek, A. Brachmann, P. Bucksbaum, R. Coffee, F. J. Decker, Y. Ding, D. Dowell, S. Edstrom, A. Fisher, J. Frisch, S. Gilevich, J. Hastings, G. Hays, P. Hering, Z. Huang *et al.*, *Nat. Photon.* **4**, 641 (2010).
 - [4] B. W. J. McNeil and N. R. Thompson, *Nat. Photon.* **4**, 814 (2010).
 - [5] T. Ishikawa, H. Aoyagi, T. Asaka, Y. Asano, N. Azumi, T. Bizen, H. Ego, K. Fukami, T. Fukui, Y. Furukawa, S. Goto, H. Hanaki, T. Hara, T. Hasegawa, T. Hatsui, A. Higashiya, T. Hirono, N. Hosoda, M. Ishii, T. Inagaki *et al.*, *Nat. Photon.* **6**, 540 (2012).
 - [6] J. S. Briggs and V. Schmidt, *J. Phys. B* **33**, R1 (2000).
 - [7] T. Schneider, P. L. Chocian, and J.-M. Rost, *Phys. Rev. Lett.* **89**, 073002 (2002).
 - [8] J. Andersson, S. Zagorodskikh, A. H. Roos, O. Talaee, R. J. Squibb, D. Koulentianos, M. Wallner, V. Zhaunerchyk, R. Singh, J. H. D. Eland, J. M. Rost, and R. Feifel, *Sci. Rep.* **9**, 17883 (2019).
 - [9] S. Grundmann, F. Trinter, A. W. Bray, S. Eckart, J. Rist, G. Kastirke, D. Metz, S. Klumpp, J. Viehhaus, L. P. H. Schmidt, J. B. Williams, R. Dörner, T. Jahnke, M. S. Schöffler, and A. S. Kheifets, *Phys. Rev. Lett.* **121**, 173003 (2018).
 - [10] M. Y. Amusia, E. G. Drukarev, V. G. Gorshkov, and M. O. Kazachkov, *J. Phys. B* **8**, 1248 (1975).
 - [11] A. Y. Istomin, N. L. Manakov, A. V. Meremianin, and A. F. Starace, *Phys. Rev. Lett.* **92**, 063002 (2004).
 - [12] A. Y. Istomin, N. L. Manakov, A. V. Meremianin, and A. F. Starace, *Phys. Rev. A* **71**, 052702 (2005).
 - [13] A. G. Galstyan, O. Chuluunbaatar, Y. V. Popov, and B. Piraux, *Phys. Rev. A* **85**, 023418 (2012).
 - [14] S.-G. Chen, W.-C. Jiang, S. Grundmann, F. Trinter, M. S. Schöffler, T. Jahnke, R. Dörner, H. Liang, M.-X. Wang, L.-Y. Peng, and Q. Gong, *Phys. Rev. Lett.* **124**, 043201 (2020).
 - [15] A. Palacios, T. N. Rescigno, and C. W. McCurdy, *Phys. Rev. A* **79**, 033402 (2009).
 - [16] J. Feist, S. Nagele, R. Pazourek, E. Persson, B. I. Schneider, L. A. Collins, and J. Burgdörfer, *Phys. Rev. A* **77**, 043420 (2008).
 - [17] D. A. Horner, F. Morales, T. N. Rescigno, F. Martín, and C. W. McCurdy, *Phys. Rev. A* **76**, 030701(R) (2007).
 - [18] L. A. A. Nikolopoulos and P. Lambropoulos, *J. Phys. B* **40**, 1347 (2007).
 - [19] I. A. Ivanov and A. S. Kheifets, *Phys. Rev. A* **75**, 033411 (2007).
 - [20] E. Fomouo, G. L. Kamta, G. Edah, and B. Piraux, *Phys. Rev. A* **74**, 063409 (2006).
 - [21] A. A. Sorokin, M. Wellhöfer, S. V. Bobashev, K. Tiedtke, and M. Richter, *Phys. Rev. A* **75**, 051402(R) (2007).
 - [22] H. Hasegawa, E. J. Takahashi, Y. Nabekawa, K. L. Ishikawa, and K. Midorikawa, *Phys. Rev. A* **71**, 023407 (2005).
 - [23] P. Antoine, E. Fomouo, B. Piraux, T. Shimizu, H. Hasegawa, Y. Nabekawa, and K. Midorikawa, *Phys. Rev. A* **78**, 023415 (2008).
 - [24] H. Shimada, K. Komatsu, W. Komatsubara, T. Mizuno, S. Miyake, S. Minemoto, H. Sakai, T. Majima, S. Owada, T. Togashi, M. Yabashi, and A. Yagishita, *J. Phys. B* **52**, 065602 (2019).
 - [25] Z. Zhang, L.-Y. Peng, M.-H. Xu, A. F. Starace, T. Morishita, and Q. Gong, *Phys. Rev. A* **84**, 043409 (2011).

- [26] R. Pazourek, J. Feist, S. Nagele, E. Persson, B. I. Schneider, L. A. Collins, and J. Burgdörfer, *Phys. Rev. A* **83**, 053418 (2011).
- [27] J. Feist, R. Pazourek, S. Nagele, E. Persson, B. I. Schneider, L. A. Collins, and J. Burgdörfer, *J. Phys. B* **42**, 134014 (2009).
- [28] S. Laulan and H. Bachau, *Phys. Rev. A* **68**, 013409 (2003).
- [29] J. Feist, S. Nagele, R. Pazourek, E. Persson, B. I. Schneider, L. A. Collins, and J. Burgdörfer, *Phys. Rev. Lett.* **103**, 063002 (2009).
- [30] E. Fomouo, A. Hamido, P. Antoine, B. Piraux, H. Bachau, and R. Shakeshaft, *J. Phys. B* **43**, 091001 (2010).
- [31] W.-C. Jiang, J.-Y. Shan, Q. Gong, and L.-Y. Peng, *Phys. Rev. Lett.* **115**, 153002 (2015).
- [32] J. W. Cooper, *Phys. Rev. A* **42**, 6942 (1990).
- [33] J. W. Cooper, *Phys. Rev. A* **47**, 1841 (1993).
- [34] A. Y. Istomin, A. F. Starace, N. L. Manakov, A. V. Meremianin, A. S. Kheifets, and I. Bray, *Phys. Rev. A* **72**, 052708 (2005).
- [35] G. F. Gribakin, V. K. Ivanov, A. V. Korol, and M. Y. Kuchiev, *J. Phys. B* **32**, 5463 (1999).
- [36] D. I. R. Boll, O. A. Fojón, C. W. McCurdy, and A. Palacios, *Phys. Rev. A* **99**, 023416 (2019).
- [37] A. S. Kheifets, I. A. Ivanov, and I. Bray, *Phys. Rev. A* **76**, 025402 (2007).
- [38] I. A. Ivanov and A. S. Kheifets, *Phys. Rev. A* **79**, 023409 (2009).
- [39] S. Fritzsche, A. N. Grum-Grzhimailo, E. V. Gryzlova, and N. M. Kabachnik, *J. Phys. B* **41**, 165601 (2008).
- [40] A. N. Grum-Grzhimailo, E. V. Gryzlova, and M. Meyer, *J. Phys. B* **45**, 215602 (2012).
- [41] M. Ilchen, G. Hartmann, E. Gryzlova, V. A. Achner, E. Allaria, A. Beckmann, M. Braune, J. Buck, C. Callegari, R. N. Coffee, R. Cucini, M. Danailov, A. De Fanis, A. Demidovich, E. Ferrari, P. Finetti, L. Glaser, A. Knie, A. O. Lindahl, O. Plekan *et al.*, *Nat. Commun.* **9**, 4659 (2018).
- [42] S. Augustin, M. Schulz, G. Schmid, K. Schnorr, E. V. Gryzlova, H. Lindenblatt, S. Meister, Y. F. Liu, F. Trost, L. Fechner, A. N. Grum-Grzhimailo, S. M. Burkov, M. Braune, R. Treusch, M. Gisselbrecht, C. D. Schröter, T. Pfeifer, and R. Moshhammer, *Phys. Rev. A* **98**, 033408 (2018).
- [43] L. Varvarezos, S. Düsterer, M. D. Kiselev, R. Boll, C. Bomme, A. De Fanis, B. Erk, C. Passow, S. M. Burkov, G. Hartmann, M. Ilchen, P. Johnsson, T. J. Kelly, B. Manschwetus, T. Mazza, M. Meyer, D. Rompotis, O. Zatsarinny, E. V. Gryzlova, A. N. Grum-Grzhimailo *et al.*, *Phys. Rev. A* **103**, 022832 (2021).
- [44] J. M. Ngoko Djiokap, N. L. Manakov, A. V. Meremianin, S. X. Hu, L. B. Madsen, and A. F. Starace, *Phys. Rev. Lett.* **113**, 223002 (2014).
- [45] M. S. Pindzola, Y. Li, and J. Colgan, *J. Phys. B* **49**, 215603 (2016).
- [46] J. M. N. Djiokap and A. F. Starace, *J. Opt.* **19**, 124003 (2017).
- [47] S. Donsa, I. Březinová, H. Ni, J. Feist, and J. Burgdörfer, *Phys. Rev. A* **99**, 023413 (2019).
- [48] A. Palacios, T. N. Rescigno, and C. W. McCurdy, *Phys. Rev. Lett.* **103**, 253001 (2009).
- [49] J. Feist, S. Nagele, C. Ticknor, B. I. Schneider, L. A. Collins, and J. Burgdörfer, *Phys. Rev. Lett.* **107**, 093005 (2011).
- [50] S. Grundmann, M. Kircher, I. Vela-Perez, G. Nalin, D. Trabert, N. Anders, N. Melzer, J. Rist, A. Pier, N. Strenger, J. Siebert, P. V. Demekhin, L. P. H. Schmidt, F. Trinter, M. S. Schöffler, T. Jahnke, and R. Dörner, *Phys. Rev. Lett.* **124**, 233201 (2020).
- [51] X. Guan, K. Bartschat, and B. I. Schneider, *Phys. Rev. A* **77**, 043421 (2008).
- [52] D. A. Horner, C. W. McCurdy, and T. N. Rescigno, *Phys. Rev. A* **78**, 043416 (2008).
- [53] T. N. Rescigno and C. W. McCurdy, *Phys. Rev. A* **62**, 032706 (2000).
- [54] L. Tao, C. W. McCurdy, and T. N. Rescigno, *Phys. Rev. A* **82**, 023423 (2010).
- [55] F. L. Yip, C. W. McCurdy, and T. N. Rescigno, *Phys. Rev. A* **81**, 063419 (2010).
- [56] L.-Y. Peng and Q. Gong, *Comput. Phys. Commun.* **181**, 2098 (2010).
- [57] A. Y. Istomin, E. A. Pronin, N. L. Manakov, S. I. Marmo, and A. F. Starace, *Phys. Rev. Lett.* **97**, 123002 (2006).
- [58] S. Chelkowski, A. D. Bandrauk, and P. B. Corkum, *Phys. Rev. Lett.* **113**, 263005 (2014).